

A Bayesian Maximum Entropy Framework Using Vertical Profiles to Improve Surface Ozone Estimation From IASI+GOME2, OMI/MLS, And Cris Satellite Ozone Observations

Hantao Wang¹, Marc L. Serre¹, Kazuyuki Miyazaki², Juan Cuesta³, Jerry R. Ziemke⁴, J. Jason West¹

¹Department of Environmental Sciences and Engineering, University of North Carolina at Chapel Hill, Chapel Hill, 27599, USA

²Jet Propulsion Laboratory, California Institute of Technology, Pasadena, 91125, USA

³Univ. Paris Est Créteil and Université de Paris Cité, CNRS, LISA, 94010 Créteil, France

⁴NASA Goddard Space Flight Center, Greenbelt, 20771, USA

Correspondence to: J. Jason West (jasonwest@unc.edu)

SUPPLEMENTARY INFORMATION

Section S1. BME Covariance model

The covariance derived from the offset removed observations can be described by the following equations. Let C_X is covariance model, r is the spatial lag in degrees.

Spatial Covariance for 0-3km column ozone:

$$C_X(r) = 81.38(0.40\exp(-3r/5) + 0.60\exp(-3r/50)) \quad (S1)$$

Spatial Covariance for surface to 0-3km column ratio:

$$C_X(r) = 0.026(0.70\exp(-3r/1) + 0.30\exp(-3r/60)) \quad (S2)$$

Spatial Covariance for tropospheric column ozone:

$$C_X(r) = 69.93(0.70\exp(-3r/10) + 0.30\exp(-3r/53)) \quad (S3)$$

Spatial Covariance for Log-transformed surface to tropospheric column ratio:

$$C_X(r) = 0.091(0.68\exp(-3r/1.8) + 0.32\exp(-3r/31)) \quad (S4)$$

Section S2. Deseasonal trend method

To estimate the long-term trend in the BME-adjusted surface ozone estimates from OMI/MLS, this method first isolates and removes the seasonal cycles by fitting a harmonic regression model. Using the whole time period (2005–2022), we model the seasonal effect $S(m)$, for any given month, using a combination of 12-month and 6-month sine and cosine waves:

$$S(m) = \beta_0 + \beta_1 \sin\left(\frac{2\pi m}{12}\right) + \beta_2 \cos\left(\frac{2\pi m}{12}\right) + \beta_3 \sin\left(\frac{2\pi m}{6}\right) + \beta_4 \cos\left(\frac{2\pi m}{6}\right) \quad (S5)$$

By calculating this seasonal effect and subtracting it from the actual observed value each month, we generate a series of monthly anomalies without the seasonal effect. Once the seasonal effects are removed, we evaluate the long-term trend on those remaining

anomalies using a median quantile regression ($\tau = 0.5$). Unlike standard linear regression, which tracks the mean, this approach models the conditional median of the anomalies over the time period (in this study is from 2005-2022).

Table S1. List of ozonesonde and IAGOS locations selected for this study. Day/Month represents the average number of recording days per month.

Type	Station	Record year	Longitude	Latitude	Day/Month
IAGOS	ABV	2015-2022	7.32	9.06	5.30
IAGOS	ADD	2012-2017	38.80	8.97	5.00
IAGOS	ATL	2005-2021	-84.42	33.68	6.40
IAGOS	BKK	2006-2023	100.64	13.81	9.53
IAGOS	BOM	2015-2023	72.94	19.12	5.00
IAGOS	CCS	2005-2017	-66.90	10.76	6.78
IAGOS	COO	2018-2022	2.40	6.51	5.00
IAGOS	CPT	2017-2020	18.56	-33.96	4.60
IAGOS	DEL	2005-2022	77.07	28.50	5.80
IAGOS	DFW	2006-2017	-96.98	33.01	6.28
IAGOS	GIG	2012-2013	-43.30	-22.70	5.30
IAGOS	HKG	2005-2023	113.95	22.15	10.42
IAGOS	HND	2018-2023	139.88	35.44	5.67
IAGOS	HYD	2006-2008	78.26	17.44	7.06
IAGOS	IAH	2017-2017	-95.25	30.00	4.00
IAGOS	IKA	2013-2023	51.16	35.43	5.40
IAGOS	JED	2012-2018	39.05	21.71	6.71
IAGOS	JFK	2005-2023	-73.61	40.59	4.00
IAGOS	KIX	2005-2023	135.08	34.40	8.81
IAGOS	KRT	2012-2014	32.64	15.48	6.13
IAGOS	KUL	2005-2016	101.64	2.84	4.82
IAGOS	KWI	2012-2022	48.03	29.35	5.21
IAGOS	LAD	2009-2013	13.29	-8.96	5.75
IAGOS	LAX	2005-2023	-118.38	33.92	10.47
IAGOS	LFW	2017-2018	1.31	6.33	4.00
IAGOS	LOS	2015-2023	3.41	6.59	4.71
IAGOS	MAA	2012-2018	80.03	13.14	7.00
IAGOS	MCT	2013-2013	58.04	23.60	5.00
IAGOS	MEL	2016-2018	144.78	-37.55	1.14
IAGOS	MNL	2015-2023	120.98	14.53	5.56
IAGOS	NBO	2019-2022	36.89	-1.34	4.00
IAGOS	NIM	2013-2018	2.13	13.50	5.00
IAGOS	NKC	2017-2022	-15.91	18.33	4.00
IAGOS	NRT	2005-2023	140.47	35.76	9.30
IAGOS	ORD	2006-2021	-87.73	42.15	9.19
IAGOS	OUA	2013-2018	-1.33	12.56	4.75
IAGOS	PHC	2015-2022	7.01	5.30	5.33
IAGOS	PTY	2017-2020	-79.22	9.15	4.80
IAGOS	SFO	2005-2018	-122.35	37.68	5.44
IAGOS	SGN	2005-2018	106.62	10.84	5.53

IAGOS	SIN	2012-2018	104.02	1.42	6.17
IAGOS	SJO	2014-2023	-84.35	9.94	2.23
IAGOS	SSG	2015-2022	8.46	3.93	4.33
IAGOS	SYD	2016-2018	151.23	-33.92	5.00
IAGOS	THR	2005-2005	51.31	35.65	7.13
IAGOS	TLV	2010-2012	34.66	32.09	4.67
IAGOS	TPE	2012-2023	121.11	25.03	18.71
IAGOS	WDH	2005-2013	17.48	-22.39	13.49
Ozonesonde	alert	2005-2024	-62.30	82.50	4.69
Ozonesonde	ascension	2005-2022	-14.22	-7.56	4.41
Ozonesonde	boulder	2005-2023	-105.20	39.95	4.92
Ozonesonde	broadmeadows	2005-2024	144.95	-37.69	4.36
Ozonesonde	churchill	2005-2021	-94.07	58.75	4.52
Ozonesonde	costarica	2005-2021	-84.21	9.98	4.66
Ozonesonde	davis	2006-2024	77.97	-68.58	4.30
Ozonesonde	debilt	2005-2020	5.18	52.10	4.58
Ozonesonde	easter island	2005-2015	-109.42	-27.17	4.08
Ozonesonde	edmonton	2005-2021	-114.10	53.54	4.50
Ozonesonde	eureka	2005-2020	-86.42	80.05	6.08
Ozonesonde	fiji	2008-2015	178.45	-18.15	4.00
Ozonesonde	goosebay	2005-2021	-60.30	53.32	4.72
Ozonesonde	hanoi	2006-2018	105.80	21.02	6.33
Ozonesonde	hilo	2005-2023	-155.05	19.72	4.31
Ozonesonde	hohenpeissenberg	2005-2023	11.00	47.80	10.62
Ozonesonde	izana	2005-2022	-16.26	28.46	4.34
Ozonesonde	kelowna	2005-2017	-119.40	49.93	5.18
Ozonesonde	kualalumpur	2005-2016	101.70	2.73	1.94
Ozonesonde	laquila	2018-2020	13.31	42.38	5.00
Ozonesonde	lauder	2005-2023	169.68	-45.04	4.61
Ozonesonde	legionowo	2005-2022	20.97	52.40	4.70
Ozonesonde	lerwick	2005-2022	-1.19	60.14	4.40
Ozonesonde	lindenberg	2014-2024	14.12	52.21	4.84
Ozonesonde	macquarie island	2005-2024	158.94	-54.50	4.34
Ozonesonde	madrid	2005-2022	-3.58	40.47	4.32
Ozonesonde	naha	2009-2018	127.69	26.21	4.19
Ozonesonde	nyalesund	2005-2022	11.95	78.93	6.64
Ozonesonde	ohp	2005-2023	5.71	43.94	4.40
Ozonesonde	paramaribo	2005-2021	-55.21	5.81	4.28
Ozonesonde	payerne	2005-2022	6.94	46.81	12.70
Ozonesonde	resolute	2005-2021	-94.98	74.72	5.12
Ozonesonde	reunion	2005-2022	55.50	-21.10	4.20
Ozonesonde	samoa	2005-2023	-170.71	-14.33	4.22
Ozonesonde	sancristobal	2005-2022	-89.60	-0.92	4.42
Ozonesonde	sapporo	2010-2018	141.33	43.06	4.22
Ozonesonde	scoresbysund	2005-2020	-21.95	70.48	4.67
Ozonesonde	sodankyla	2005-2021	26.62	67.36	4.87

Ozonesonde	trinidadhead	2005-2023	-124.15	41.06	5.05
Ozonesonde	ucclle	2005-2022	4.21	50.48	11.84
Ozonesonde	ushuaia	2008-2024	-68.31	-54.85	4.70
Ozonesonde	valentia	2006-2022	-10.25	51.93	4.35
Ozonesonde	wallops	2005-2020	-75.70	37.90	4.59
Ozonesonde	yarmouth	2005-2021	-66.11	43.87	4.84

Table S2. Satellite observations used for ozone assimilation in TCR-2. Table based on Miyazaki et al. (2020)

Species	Instrument	Period	Data typea	Reference
NO ₂ , SO ₂	OMI (Aura)	2005-2020	TrC for NO ₂ , PBL for SO ₂	(Boersma et al., 2011; Boersma et al., 2017; Krotkov et al., 2016; Li et al., 2013)
NO ₂	SCIAMACHY (Envisat)	2005-2012	TrC	(Boersma et al., 2004)
NO ₂	GOME-2 (Metop-A)	2007-2020	TrC	
Ozone	TES (Aura)	2005-2011	PROF	(Bowman et al., 2006; Herman and Kulawik, 2013)
Ozone, HNO ₃	MLS (Aura)	2005-2020	PROF	(Livesey et al., 2017)
CO	MOPITT (Terra)	2005-2020	PROF	(Deeter et al., 2017; Deeter et al., 2013)

^aSatellite retrievals of atmospheric composition that were assimilated in the chemistry reanalysis. TC is total column, TRC is tropospheric column, PROF is profiles, PC is partial columns. PBL is planetary boundary layer.

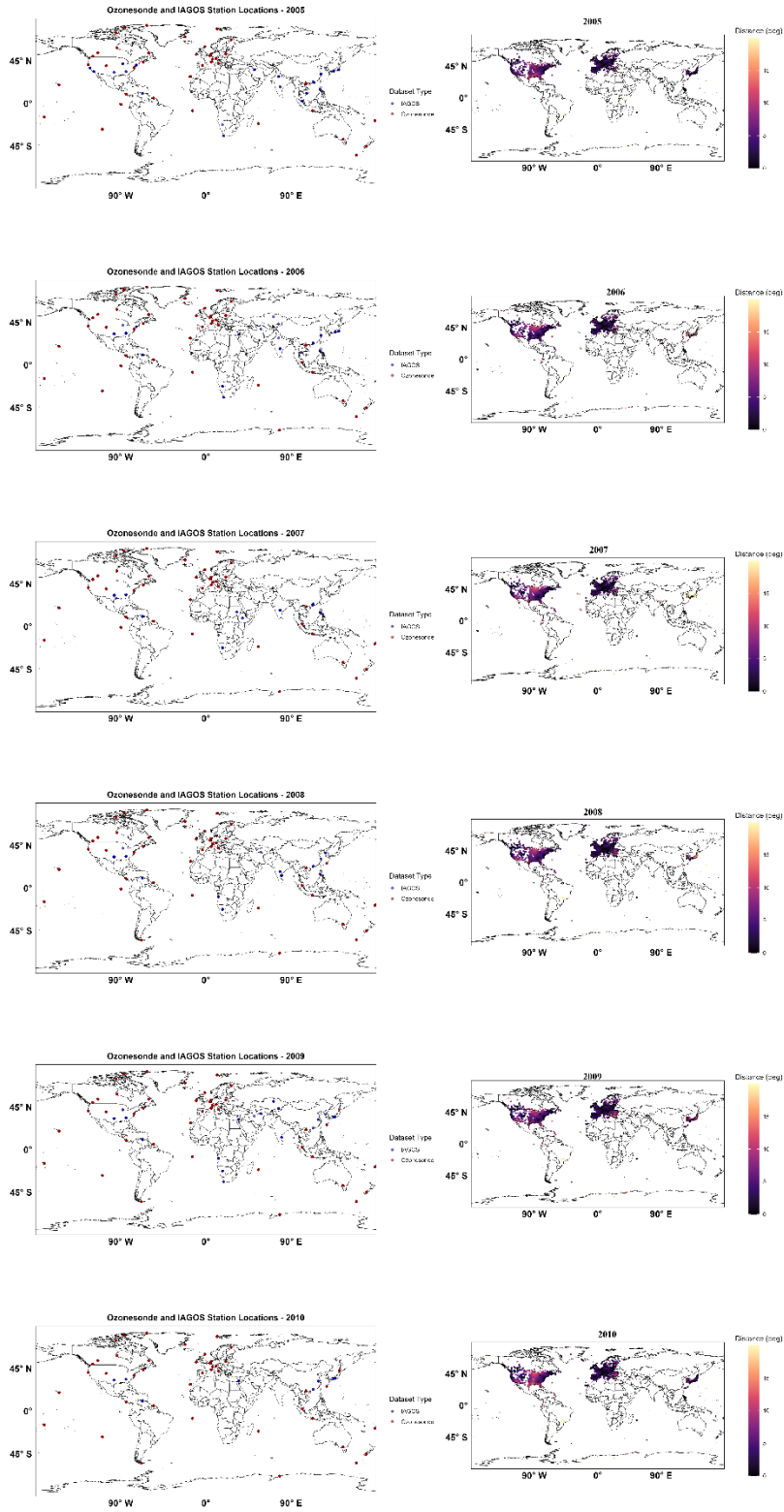
Table S3. The regions defined by Hemispheric Transport Air Pollution(HTAP)2 (Koffi et al., 2016)

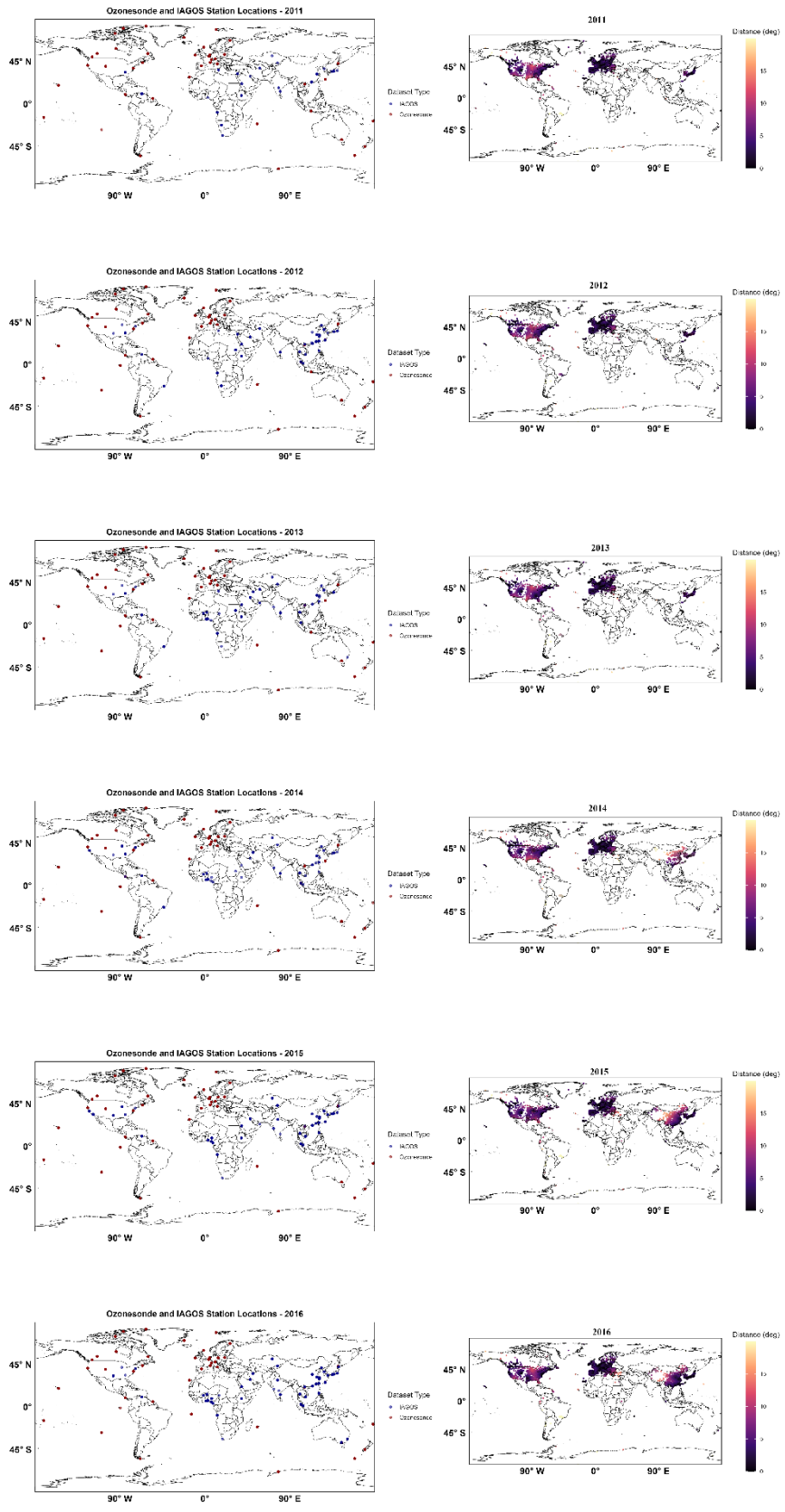
	Tier 1		Tier 2
01	GLO*	World	
02	OCN	Non-arctic/Antarctic Ocean	020 Baltic Sea 021 North Atlantic 022 South Atlantic 023 North Pacific 024 South Pacific 025 Indian Ocean 026 Hudson Bay 027 Mediterranean Sea 028 Black and Caspian Sea
03	NAM*	US+Canada (upto 66 N; polar circle)	031 NE US (all divided on state or provincial lines) 032 SE US 033 NW US 034 SW US 035 E. Canada 036 W. Canada + Alaska up to 66 N.
04	EUR*	Western + Eastern EU+Turkey (upto 66 N polar circle)	041 NW Europe 042 SW Europe (France follows provinces level at ca. 46 N). 043 Eastern Europe 044 Greece+Turkey+Cyprus

05	SAS*	South Asia: India, Pakistan, Nepal, Bangladesh, Sri Lanka	051 North India+Pakistan+Nepal+Bangladesh 052 South India+Sri Lanka 053 Indian Himalaya (above an elevation of 1500 m)
06	EAS*	E Asia: China, Korea, Japan	061 North East China 062 South East China 063 West China +Mongolia (excl. Himalaya) 064 North/South Korea 065 Japan 066 China/Tibet Himalaya (above an elevation of 1500 m)
07	SEA*	South East Asia	071 Indonesia+Malaysia+Singapore 072 Thailand+Myanmar+Vietnam
08	PAN	Pacific, Australia+ New Zealand	081 Pacific 082 Australia 083 New Zealand
09	NAF	Northern Africa	091 Egypt 092 Rest of Northern Africa
10	SAF*	Sub Saharan Africa	101 West and Central Africa: Côte d'Ivoire, Angola, Benin, Burkina Faso, Cameroon, Cape Verde, Chad, Congo Brazzaville, Democratic Republic of Congo, Equatorial Guinea, Gambia, Ghana, Guinea, Guinea Bissau, Liberia, Mali, Niger, Nigeria, Senegal, Sierra Leone and Togo 102 East Africa: Burundi, Djibouti, Eritrea, Ethiopia, Kenya, Sudan, Rwanda, Uganda, Somalia and Tanzania. 103 Southern Africa: Angola, Botswana, Lesotho, Madagascar, Malawi, Mauritius, Mozambique, Namibia, South Africa, Swaziland, Tanzania, Zambia, and Zimbabwe
11	MDE*	Middle East; S. Arabia etc, Iran, Iraq	111 Middle East 112 S.Arabia; Yemen; Oman; etc 113 Iran, Iraq
12	MCA	Mexico, Central America, Caribbean, Guyanas, Venezuela, Columbia	121 Mexico 122 Central America 123 Caribbean 124 Guyanas, Columbia, Venezuela
13	SAM	S. America	131 South Brazil 132 Rest of Brazil 133 Uruguay, Paraguay, Argentina, Chile 134 Peru, Ecuador
14	RBU	Russia, Belarussia, Ukraine, Central Asia	141 Russia West 142 Russia East 143 Belarussia+Ukraine
15	CAS	Central Asia	144 Uzbekistan, Kazakhstan, Kyrgyzstan, Tajikistan, Turkmenistan
16	NPO	Arctic Circle (North of 66 N)+Greenland	150 Arctic (includes ocean and all of Greenland)
17	SPO	Antarctic	160 Antarctic 161 Southern Ocean, south of 60S

*Regions in bold characters defined as priority regions in this paper.

Figure S1. Spatial distribution of Ozone sonde and IAGOS locations (left), and TOAR-II locations (right). The color scale indicates the distance to the nearest vertical profile site.





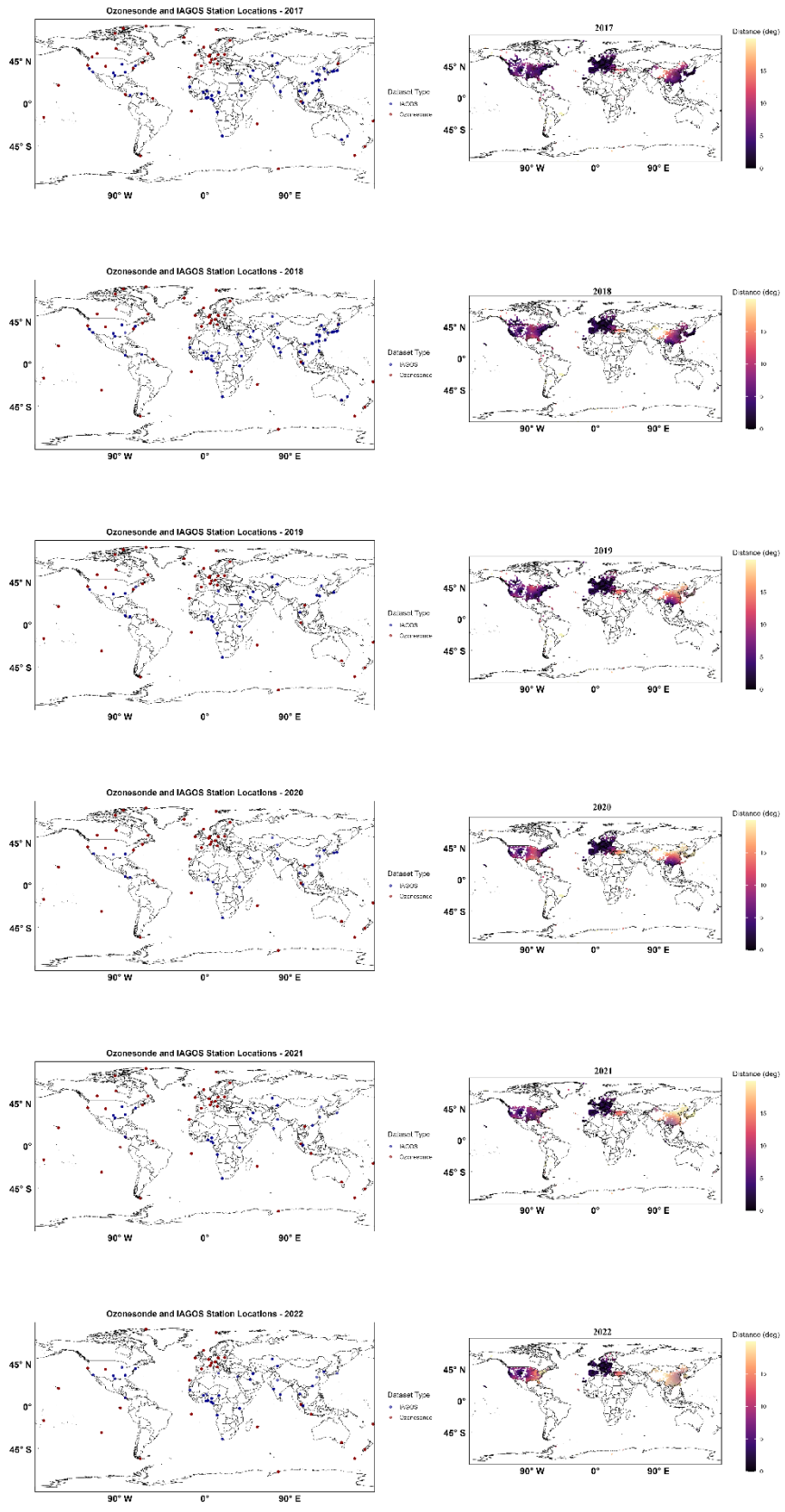
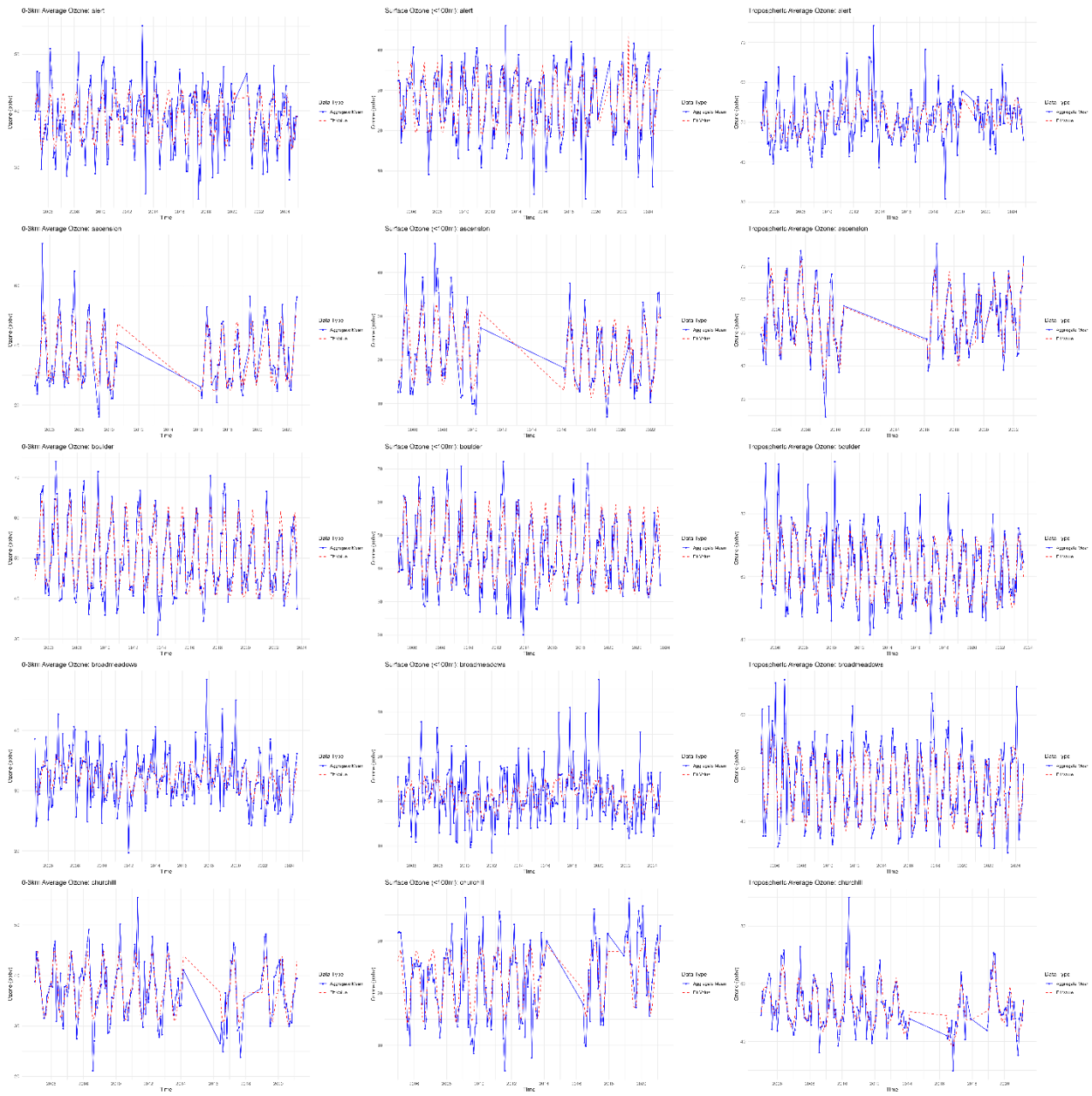
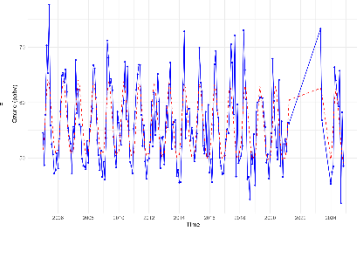
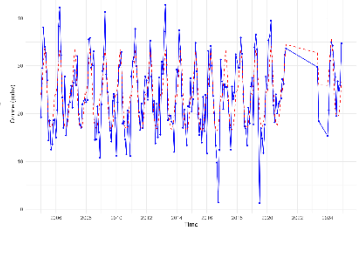
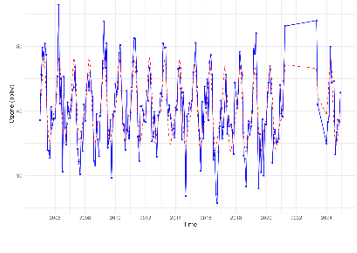
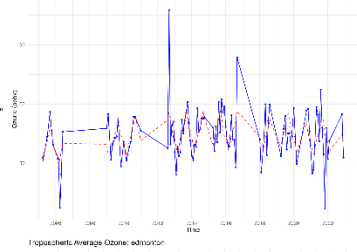
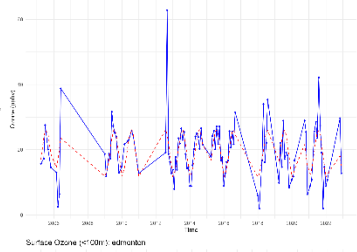
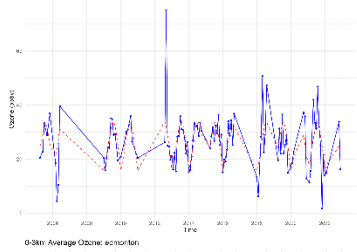
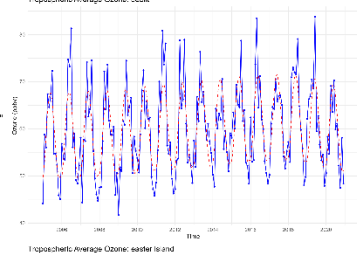
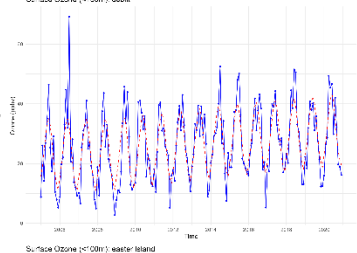
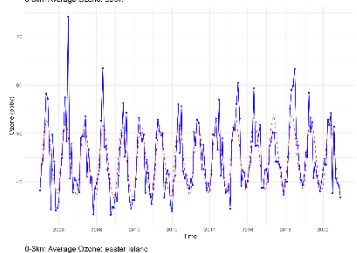
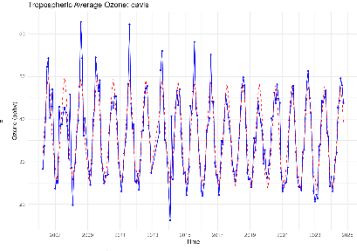
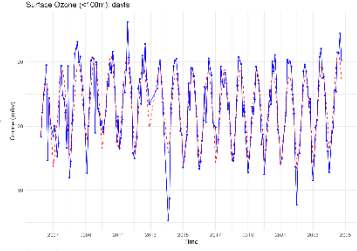
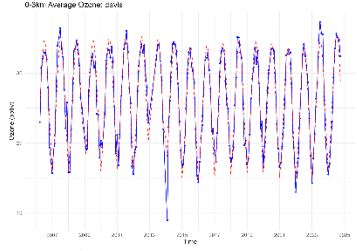
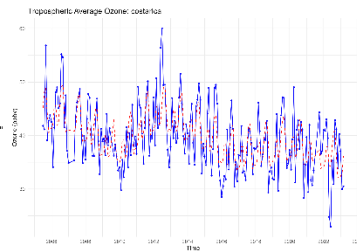
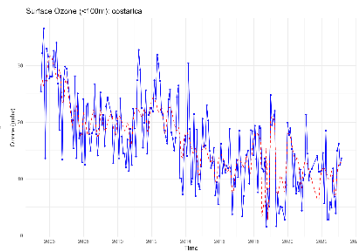
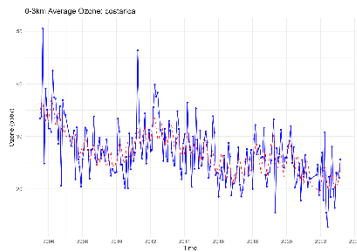
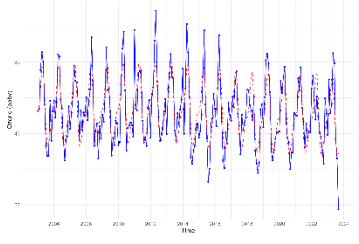
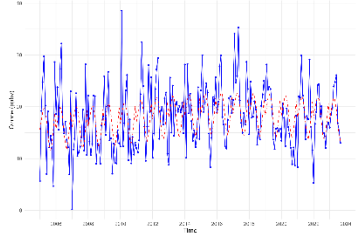
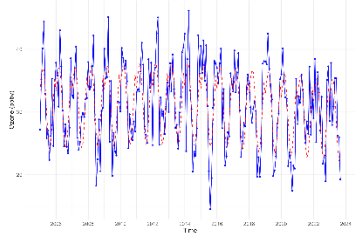
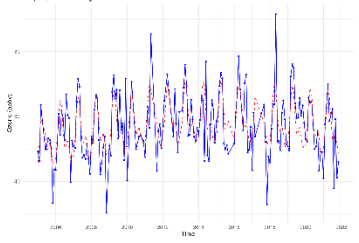
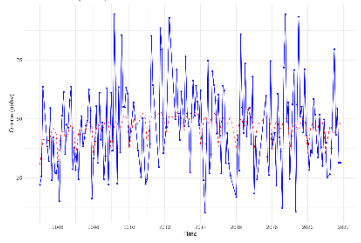
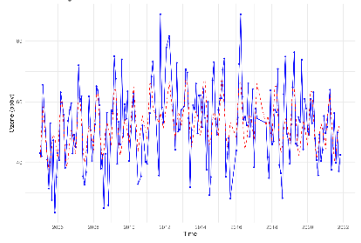
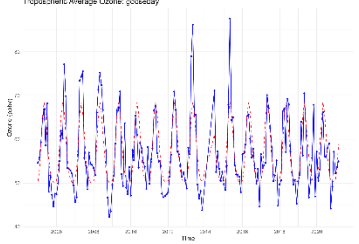
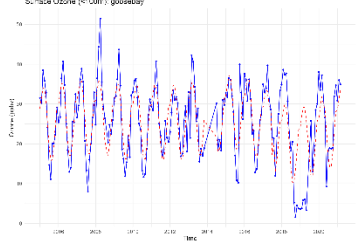
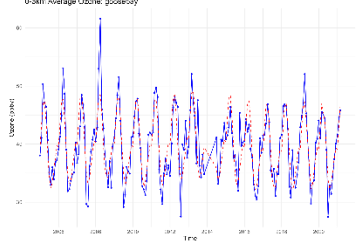
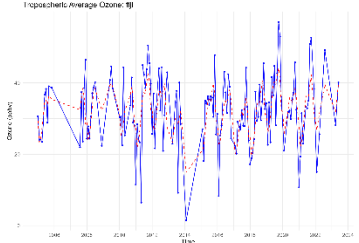
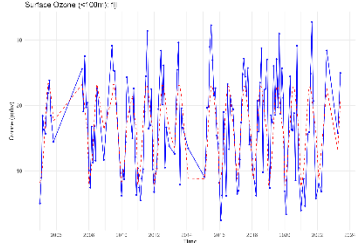
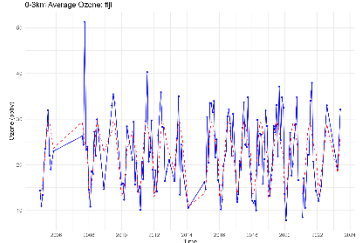
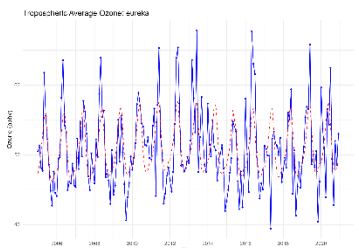
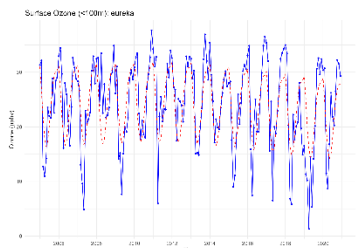
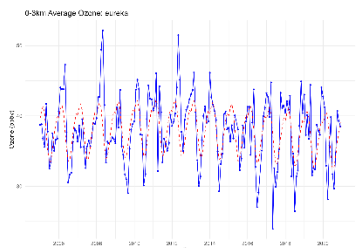
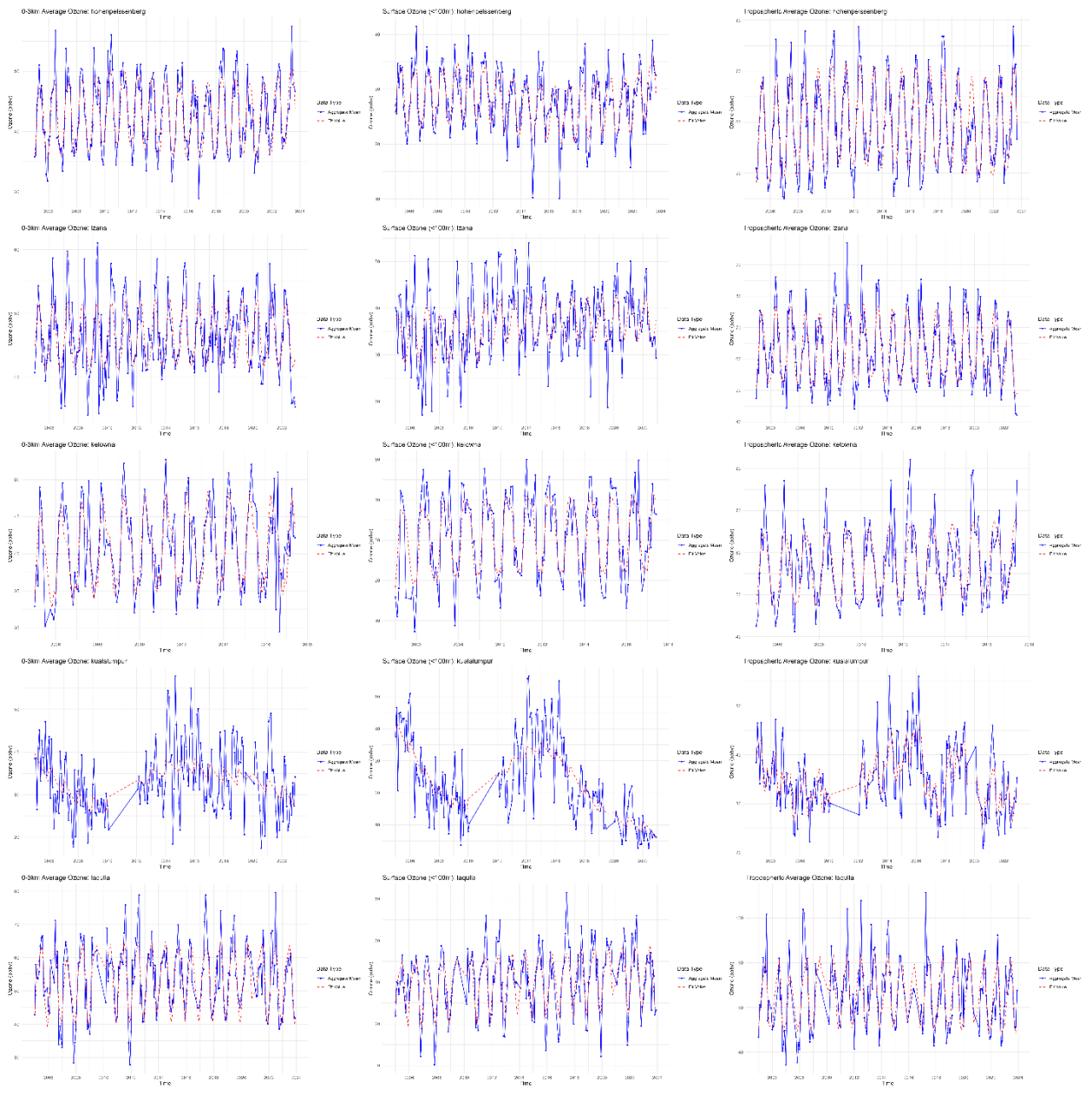


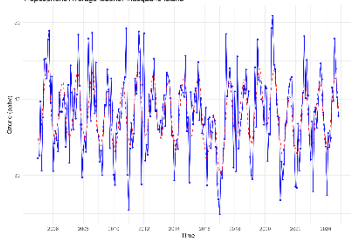
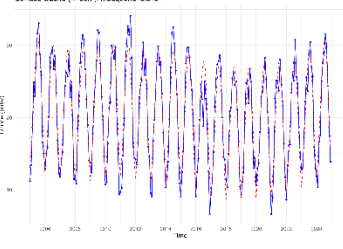
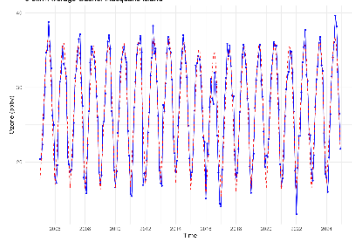
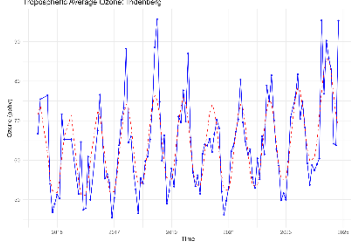
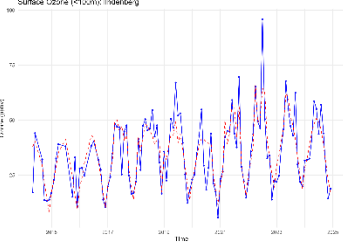
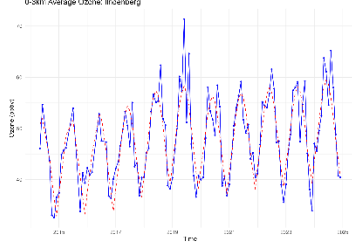
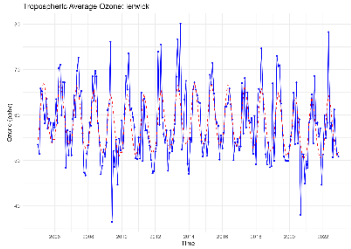
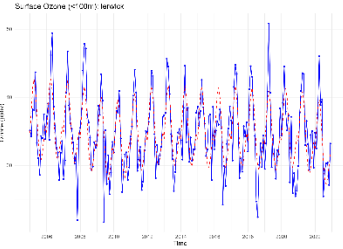
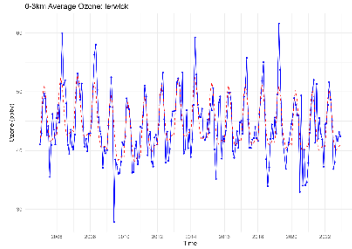
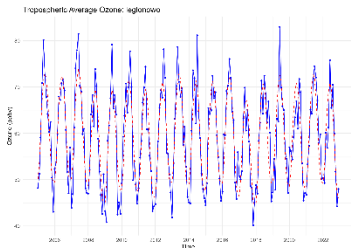
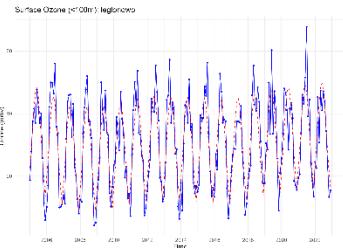
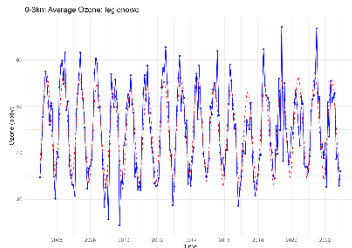
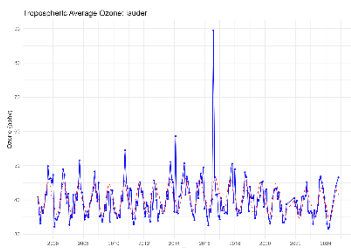
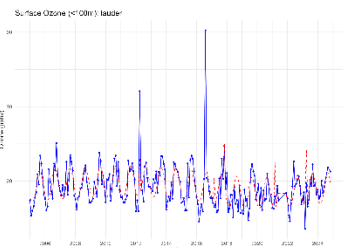
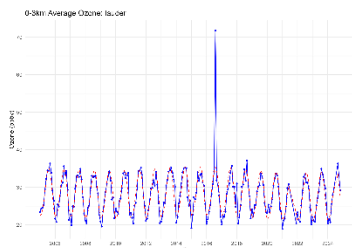
Figure S2. Time series of monthly ozone vertical profiles. The red line represents the aggregate monthly mean derived from daily records, while the blue line represents the monthly values fitted using a GAM.

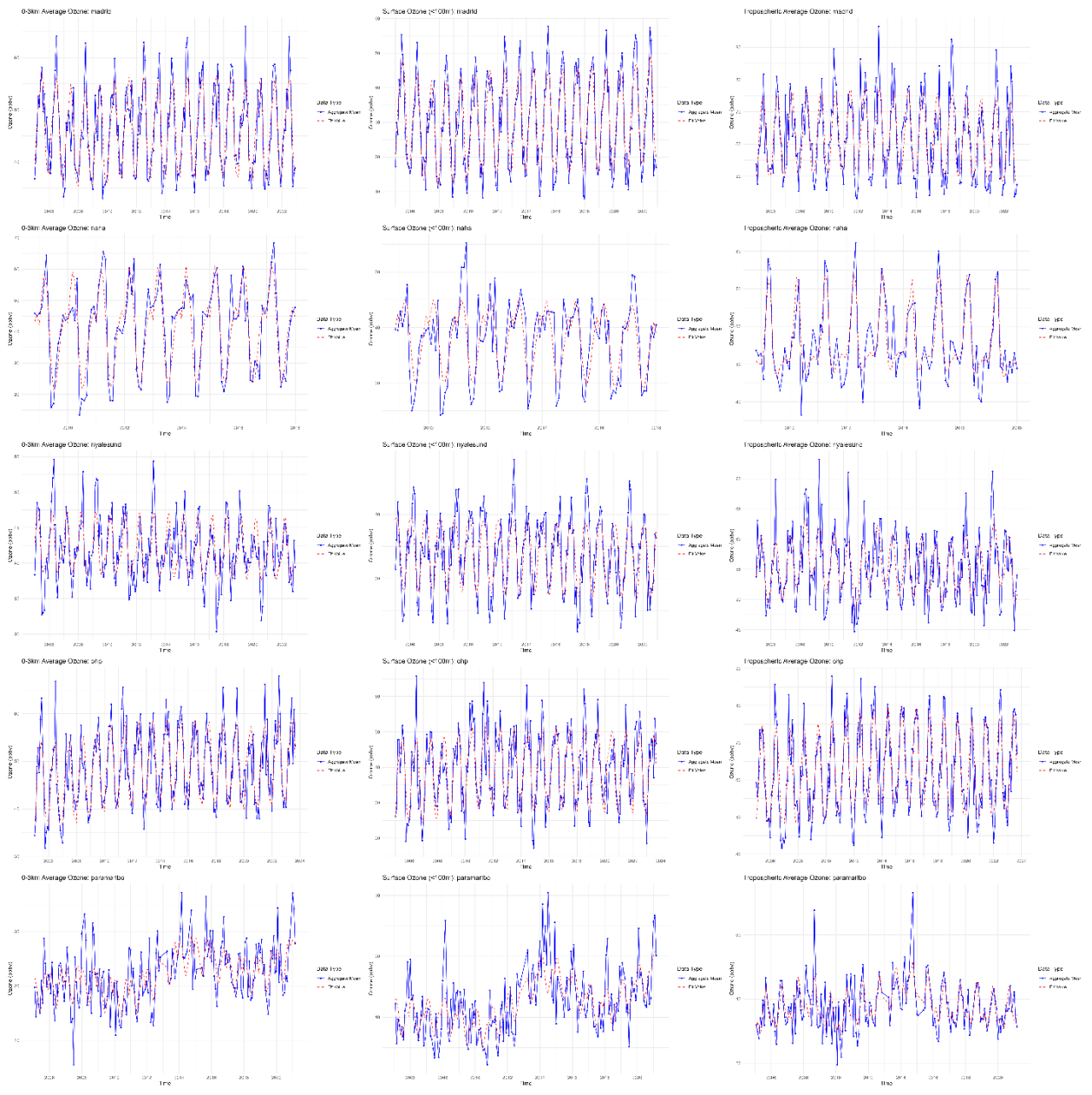


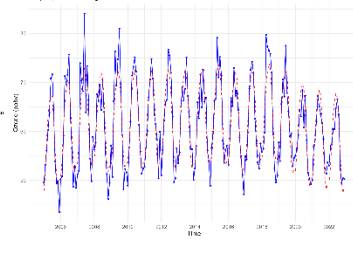
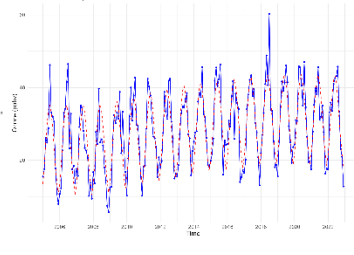
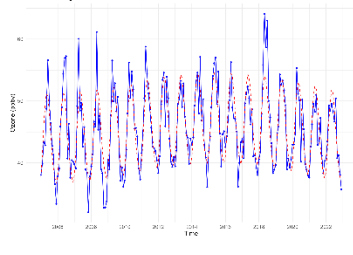
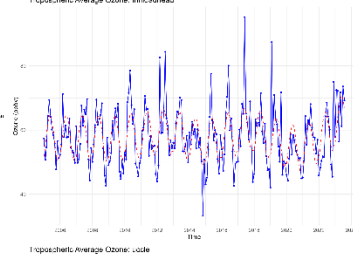
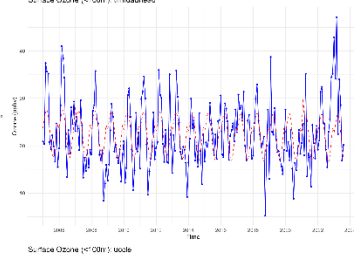
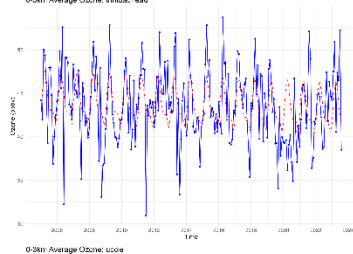
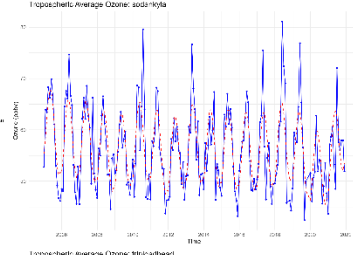
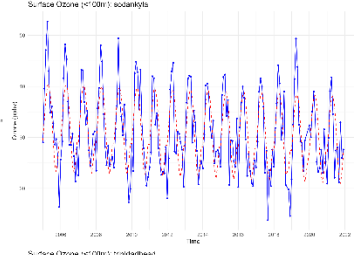
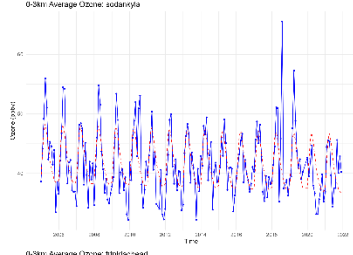
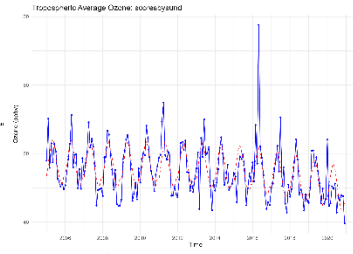
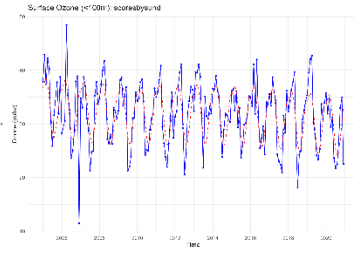
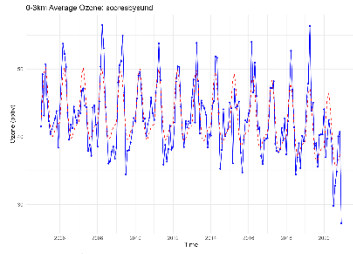
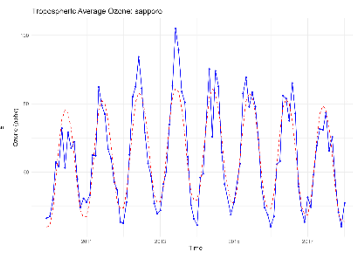
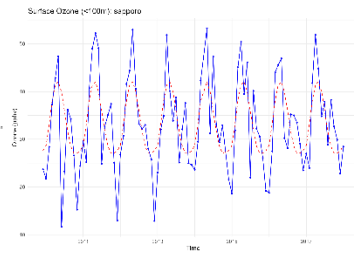
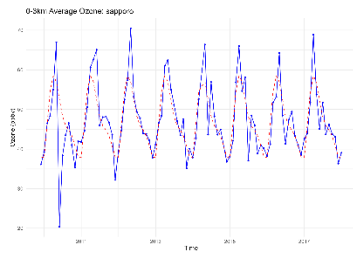


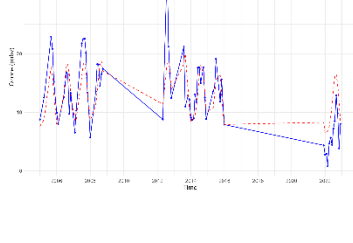
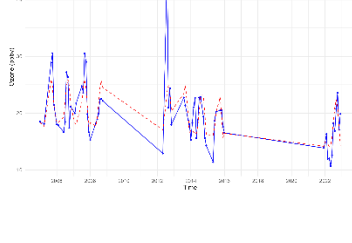
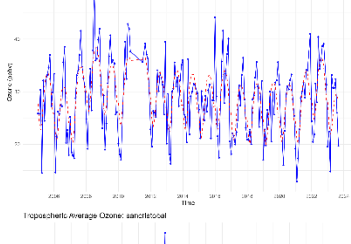
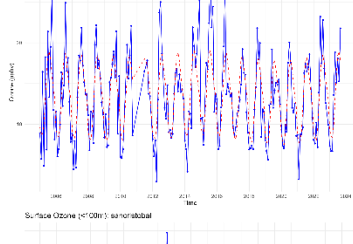
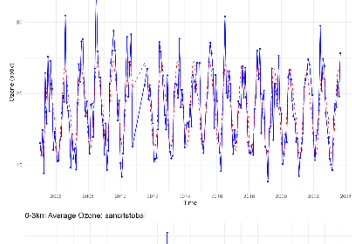
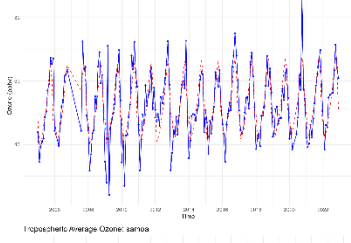
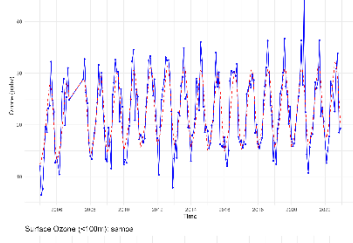
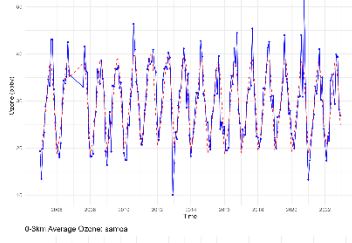
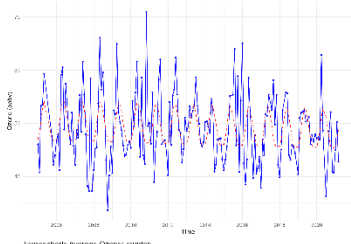
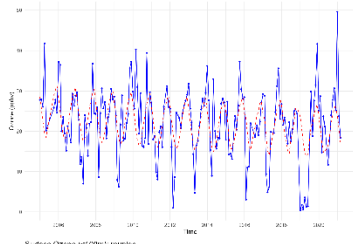
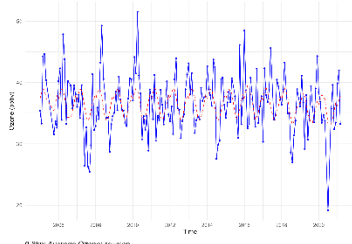
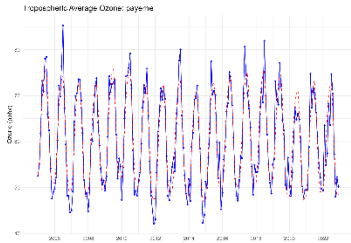
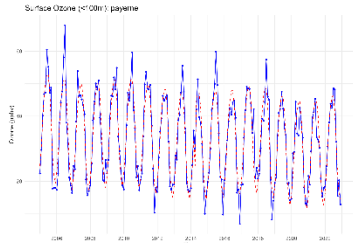
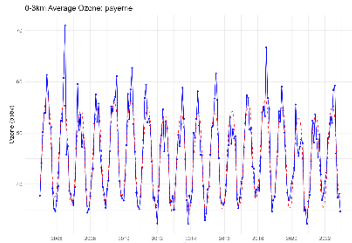


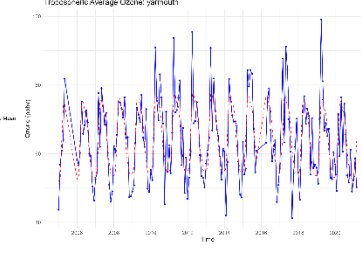
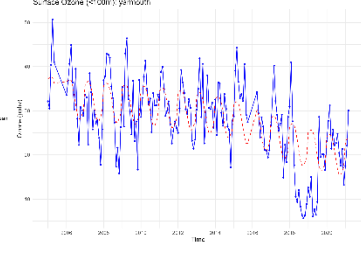
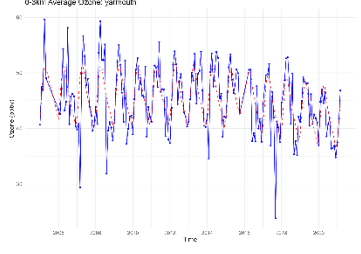
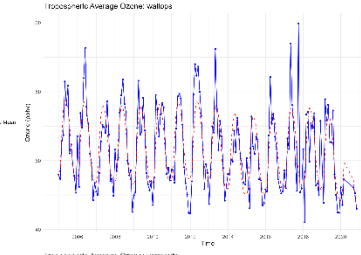
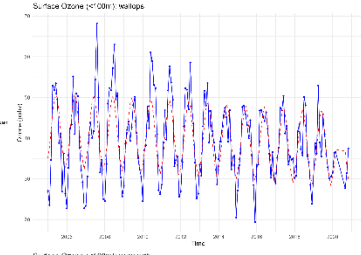
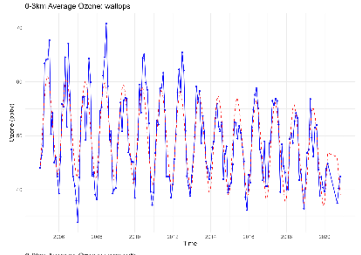
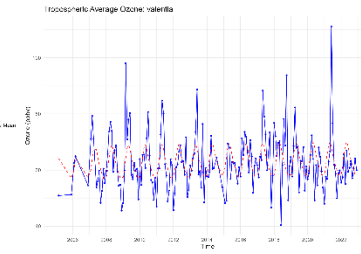
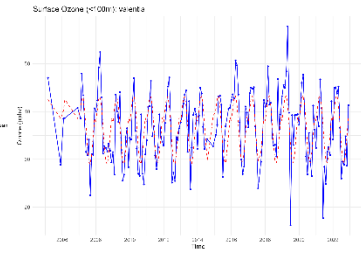
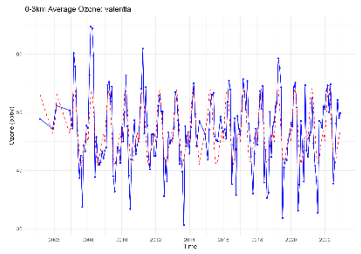
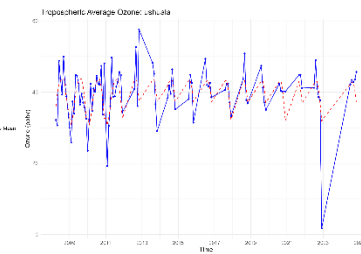
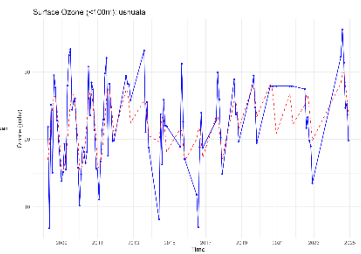
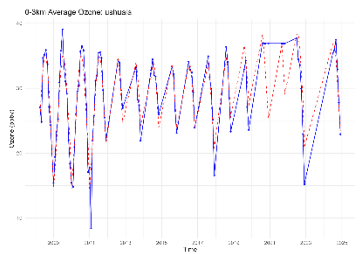












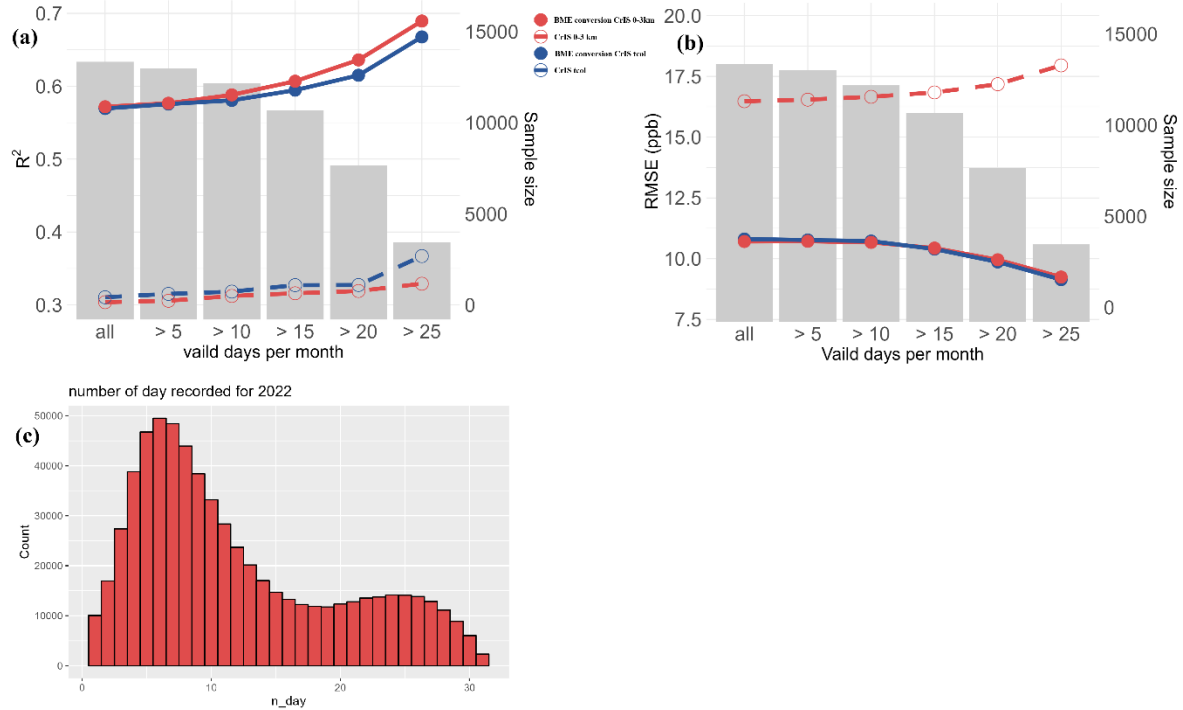


Figure S3. CrIS performance across varying daily data densities. Evaluation of the BME-adjusted conversion method for CrIS 0–3 km ozone and CrIS tropospheric column ozone against TOAR-II monthly average DMA8 ozone observations (2022): (a) spatial correlation (R^2) versus daily data density; (b) model bias (RMSE) versus daily data density; and (c) frequency of CrIS data point locations across different daily recording counts at a $1^\circ \times 1^\circ$ resolution. Red solid line represents BME-adjusted surface ozone (from CrIS 0-3km), red dash line represents original satellite observation from CrIS 0-3km, blue solid line represents BME-adjusted surface ozone (from CrIS tropospheric column ozone), blue dash line represents original satellite observation from CrIS tropospheric column ozone.

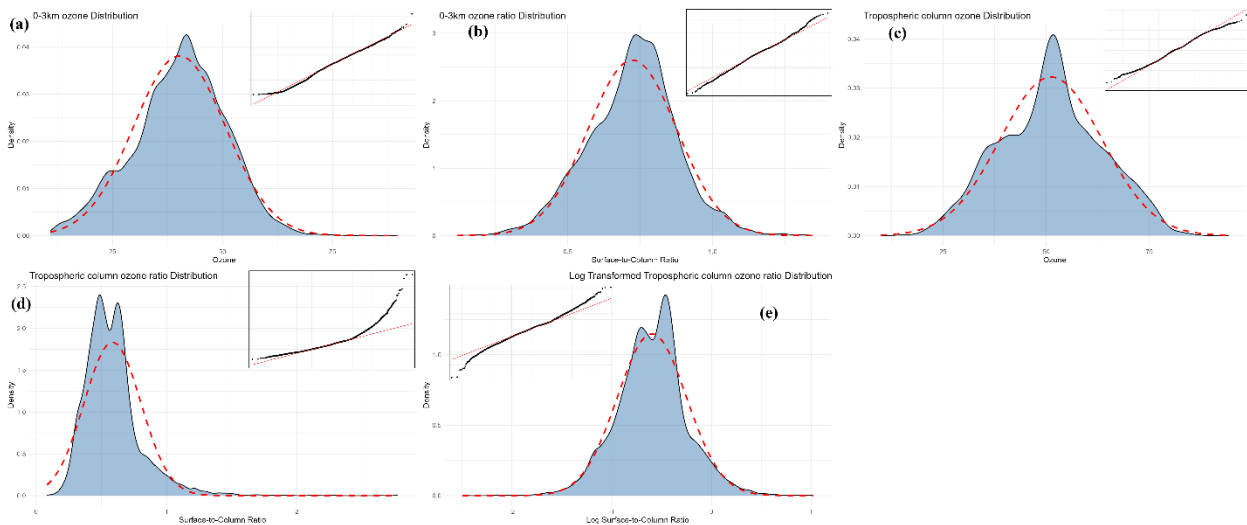


Figure S4. Normality diagnostics for variables prior to BME: (a) 0–3 km ozone; (b) 0–3 km ozone ratio; (c) Tropospheric column ozone; (d) Tropospheric column ozone ratio; and (e) Log-transformed tropospheric column ozone ratio. The ratio is defined as the surface ozone divided by the column ozone.

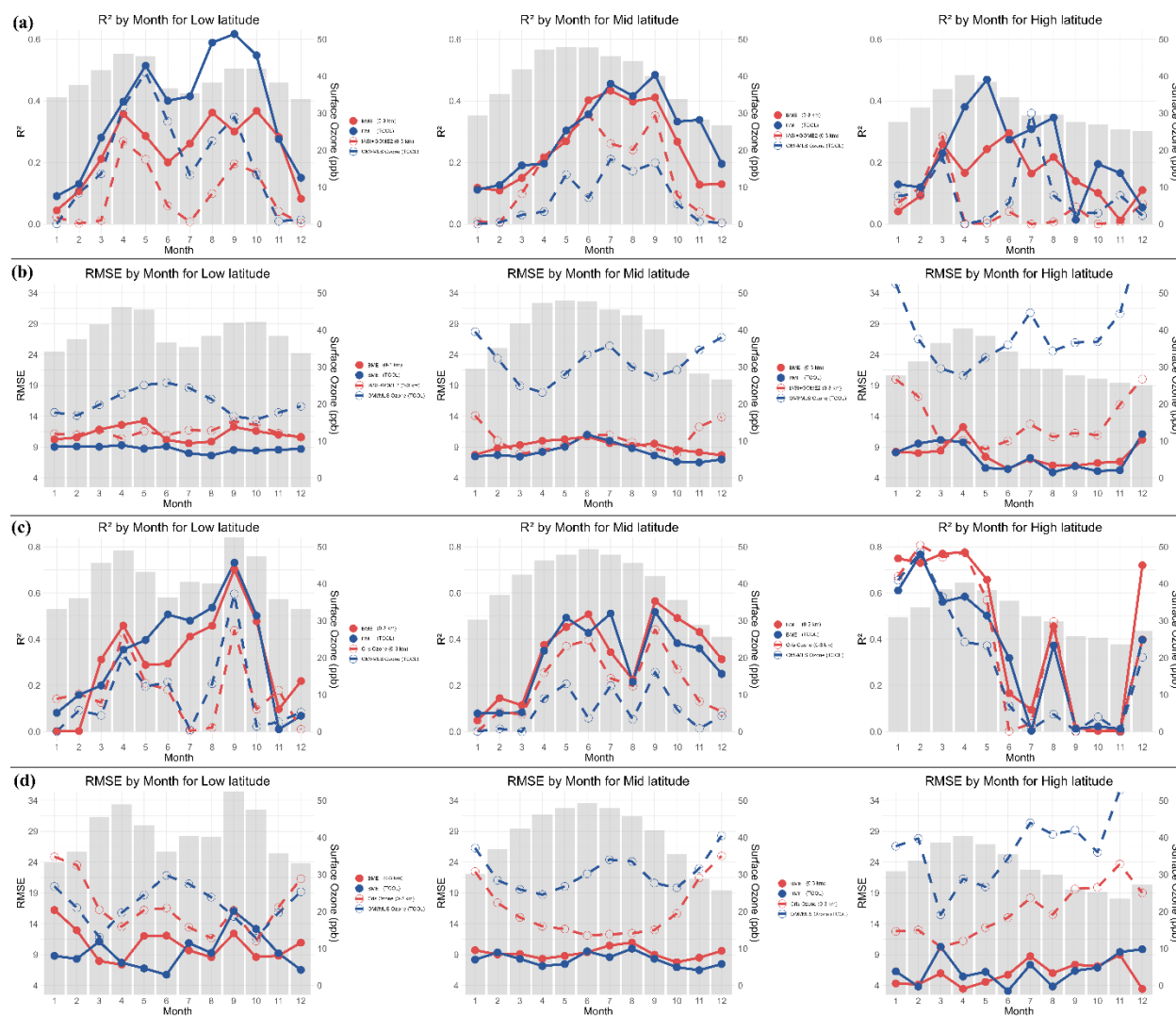


Figure S5. Monthly R^2 and RMSE of different latitude range for BME-adjusted surface ozone estimates. The evaluation includes data from IASI+GOME2 and OMI/MLS for the 2017–2020 period, and CrIS and OMI/MLS for 2022. (a) Monthly R^2 of BME-adjusted surface ozone from IASI+GOME2 and OMI/MLS 2017–2020, (b) Monthly RMSE of BME-adjusted surface ozone from IASI+GOME2 and OMI/MLS 2017–2020, (c) Monthly R^2 of BME-adjusted surface ozone from CrIS and OMI/MLS for 2022, (d) Monthly RMSE of BME-adjusted surface ozone from CrIS and OMI/MLS for 2022.

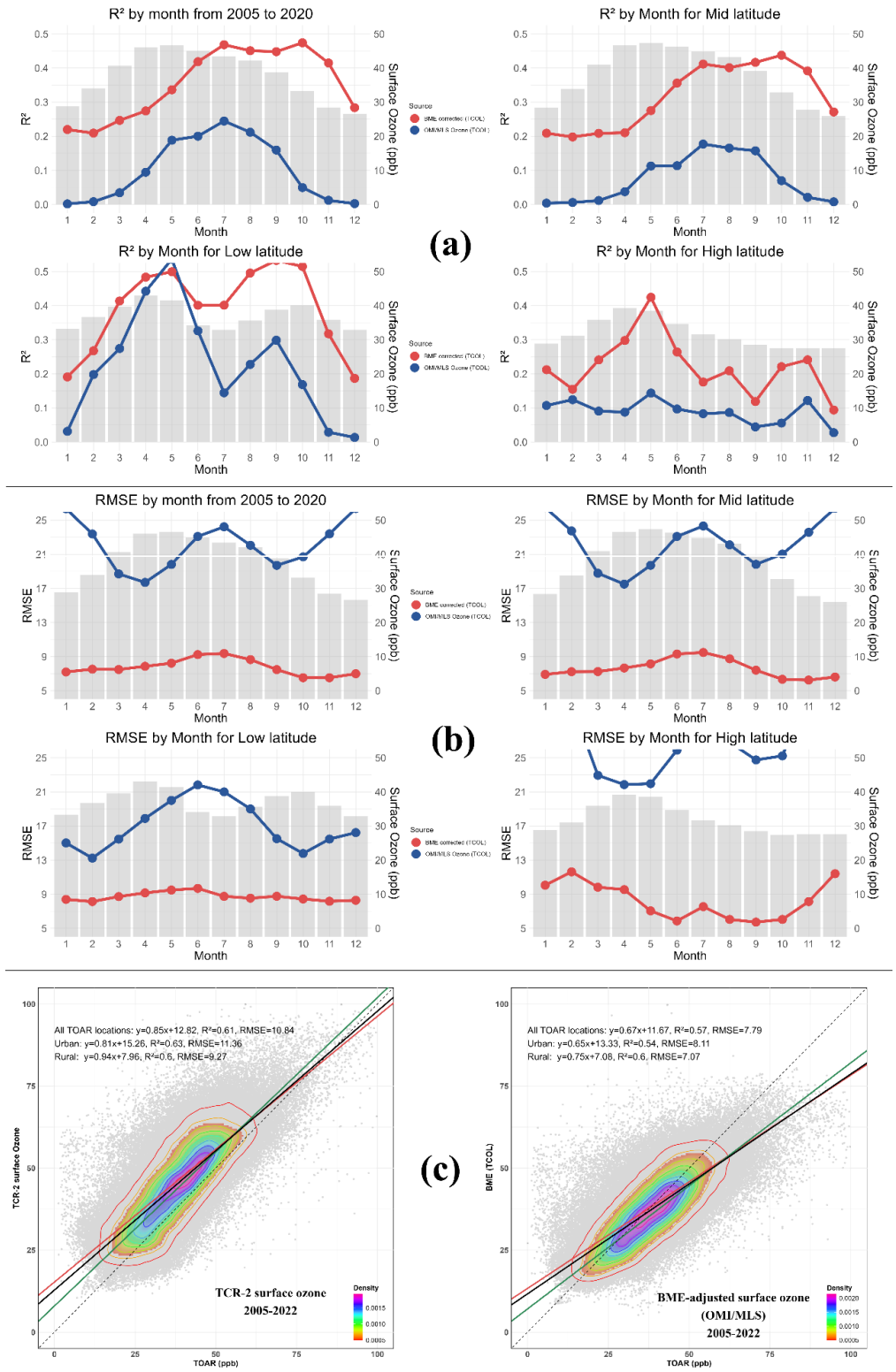


Figure S6. The evaluation is BME-adjusted surface ozone estimates from OMI/MLS for the 2005–2022 period. (a) Monthly R² of different latitude range for BME-adjusted surface ozone estimates. (b) Monthly RMSE of different latitude range for BME-adjusted surface ozone estimates. (c) OMI/MLS scatter plot with linear regression against TOAR-II.

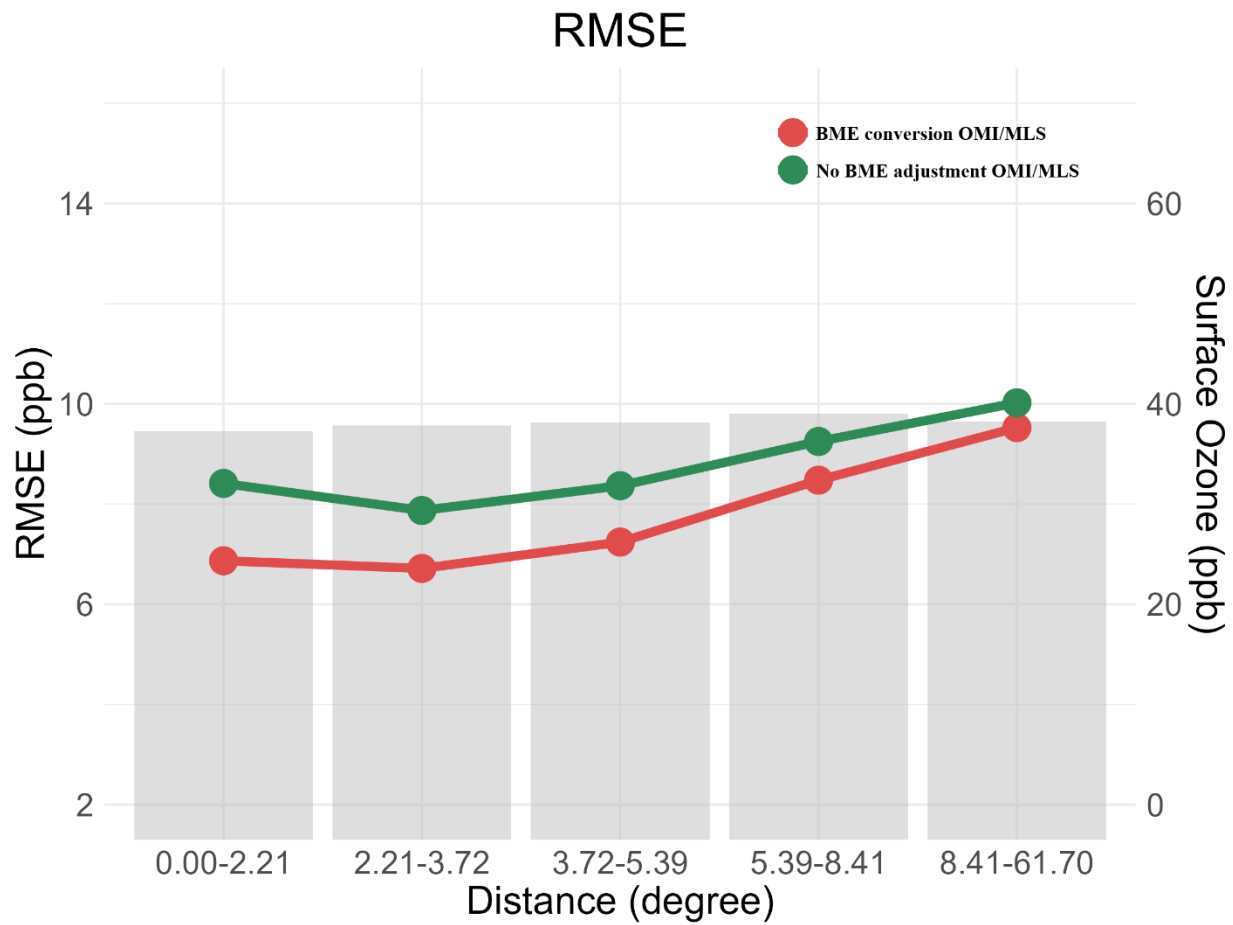
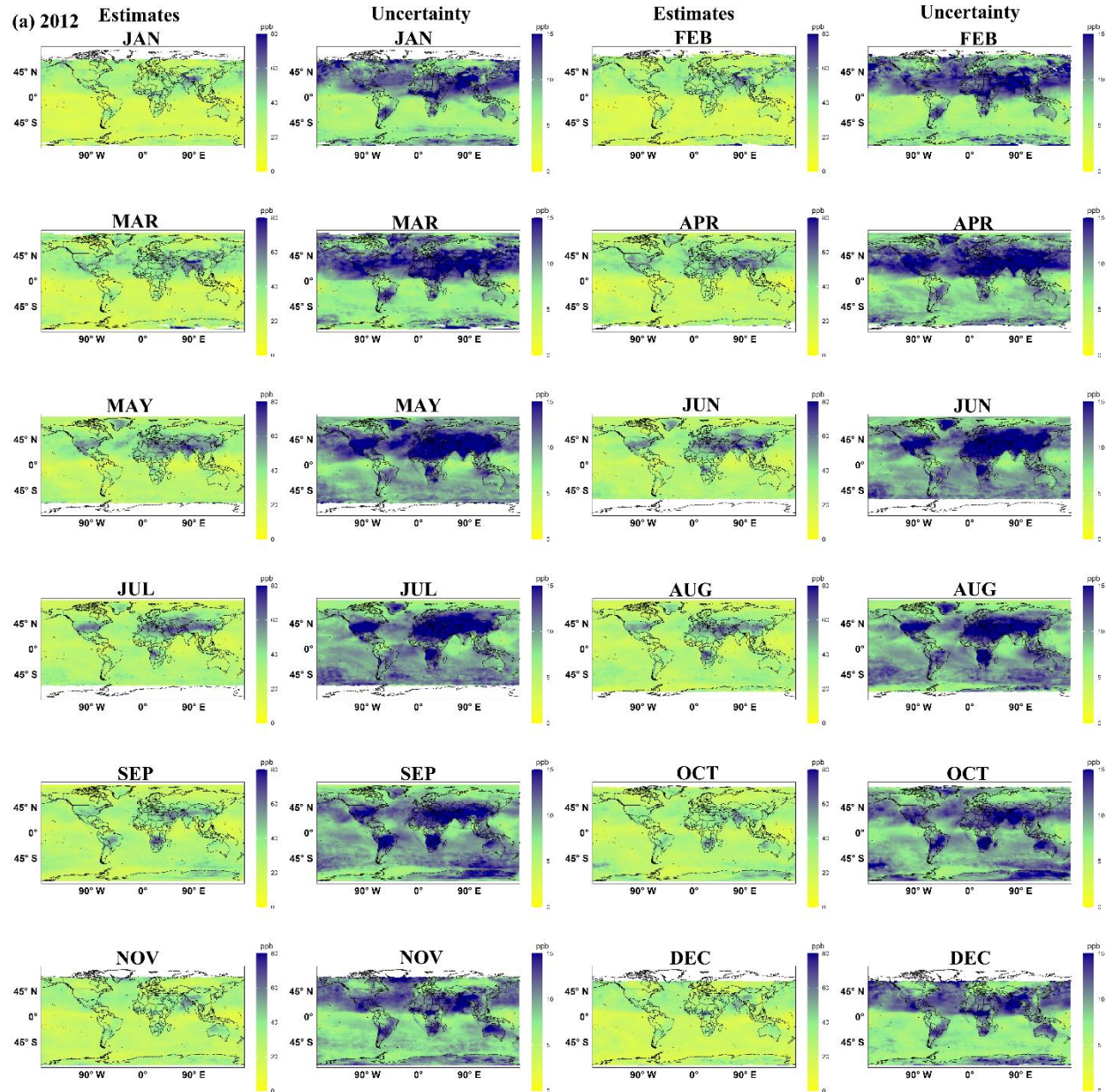
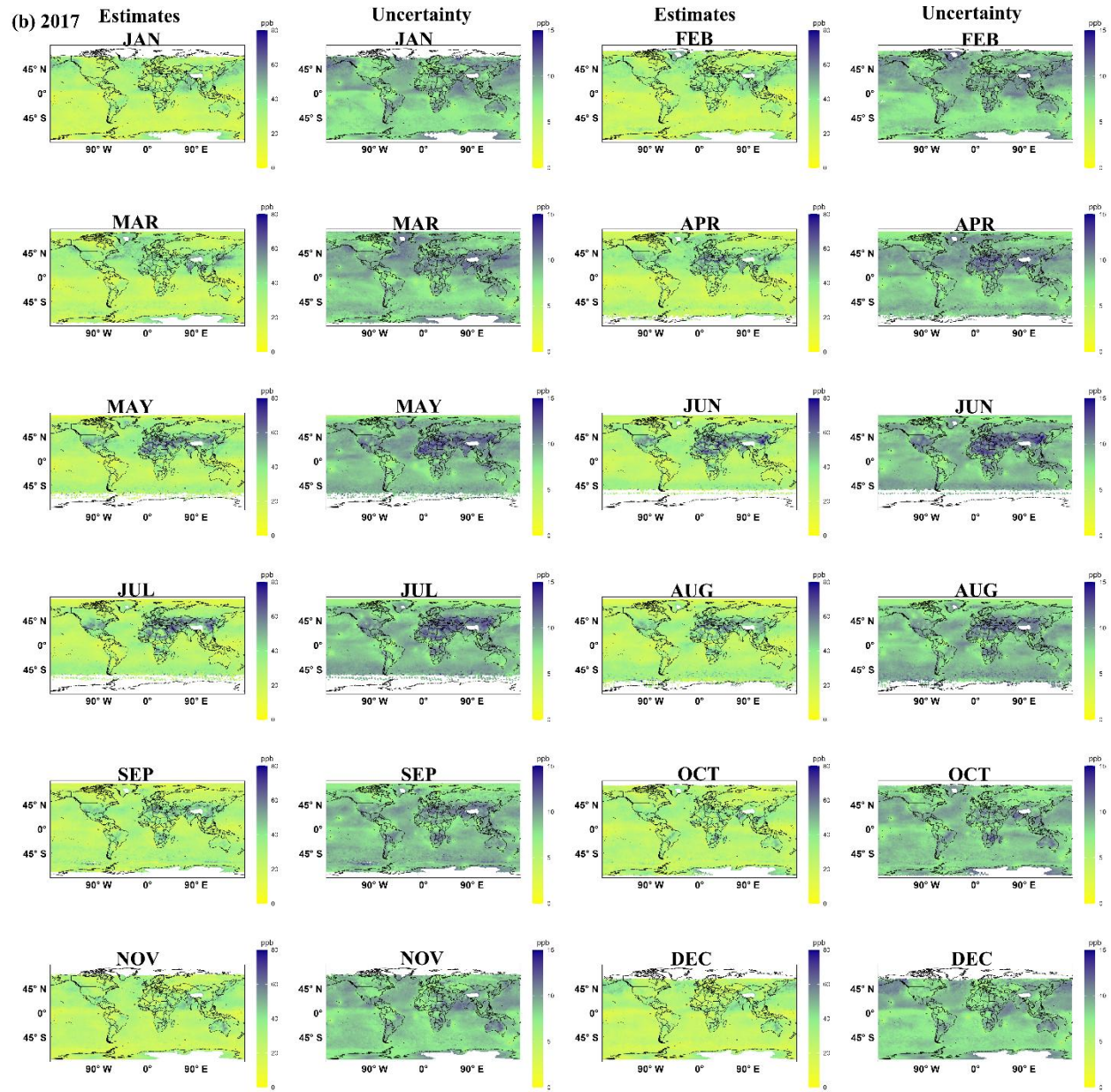
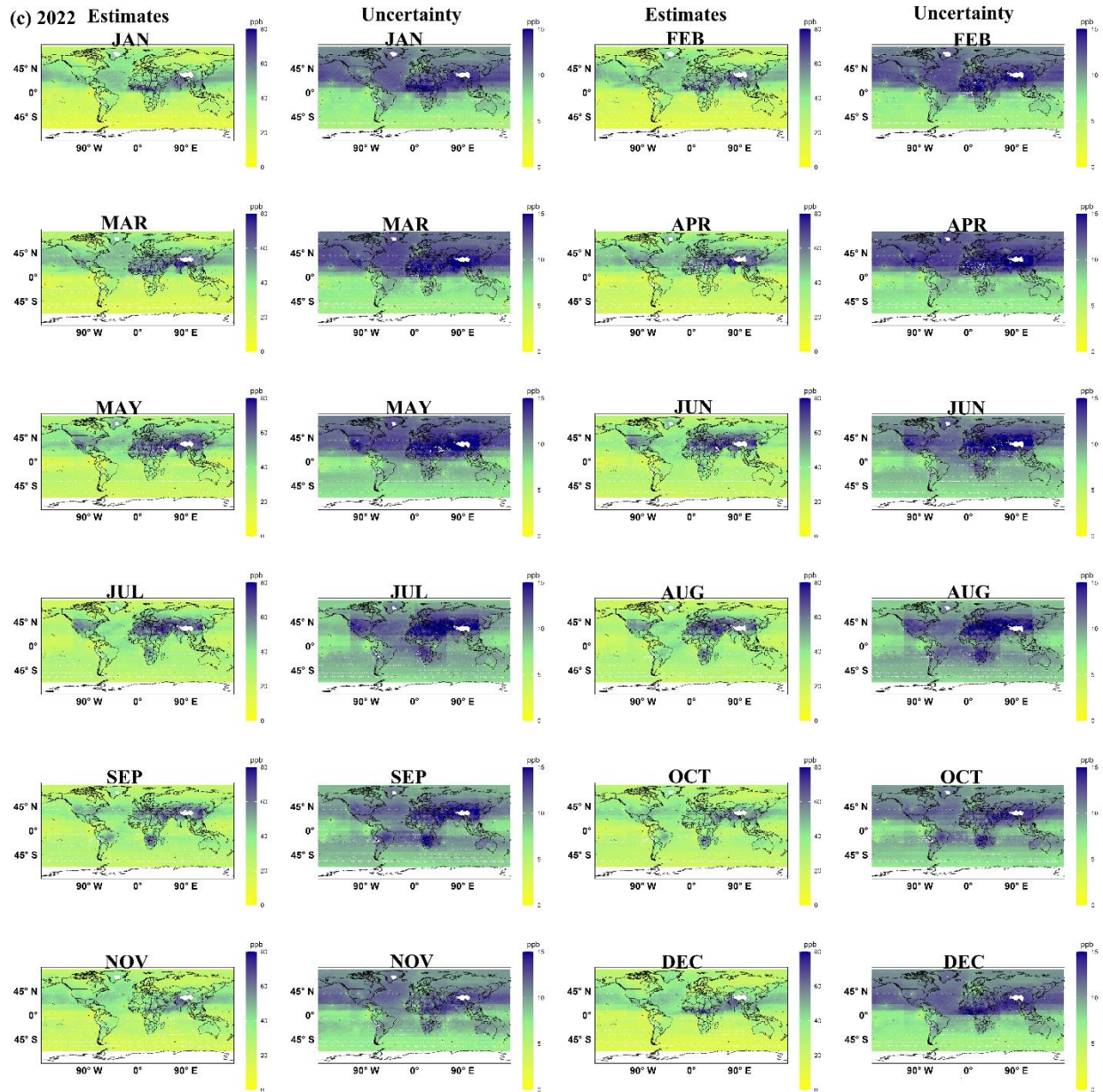


Figure S7. RMSE of BME-adjusted surface ozone from OMI/MLS data regarding the distance to the nearest vertical profile location from 2005-2022.

Figure S8. Monthly spatial distributions of BME-adjusted surface ozone estimates and corresponding uncertainty maps. The panels illustrate monthly surface ozone concentrations and their associated estimation uncertainties for three representative years: (a) 2012 (based on OMI/MLS); (b) 2017 (based on IASI+GOME-2); and (c) 2022 (based on CrIS).







Reference

- Boersma, K., Eskes, H., Richter, A., De Smedt, I., Lorente, A., Beirle, S., Van Geffen, J., Peters, E., Van Roozendaal, M., and Wagner, T.: QA4ECV NO₂ tropospheric and stratospheric vertical column data from OMI (Version 1.1)[Data set], Royal Netherlands Meteorological Institute (KNMI), 2017.
- Boersma, K. F., Eskes, H. J., and Brinksma, E. J.: Error analysis for tropospheric NO₂ retrieval from space, *Journal of Geophysical Research: Atmospheres*, 109, <https://doi.org/10.1029/2003JD003962>, 2004.
- Boersma, K. F., Eskes, H. J., Dirksen, R. J., van der A, R. J., Veefkind, J. P., Stammes, P., Huijnen, V., Kleipool, Q. L., Sneep, M., Claas, J., Leitão, J., Richter, A., Zhou, Y., and Brunner, D.: An improved tropospheric NO₂ column retrieval algorithm for the Ozone Monitoring Instrument, *Atmos. Meas. Tech.*, 4, 1905-1928, 10.5194/amt-4-1905-2011, 2011.
- Bowman, K. W., Rodgers, C. D., Kulawik, S. S., Worden, J., Sarkissian, E., Osterman, G., Steck, T., Ming, L., Eldering, A., Shephard, M., Worden, H., Lampel, M., Clough, S., Brown, P., Rinsland, C., Gunson, M., and Beer, R.: Tropospheric emission spectrometer: retrieval method and error analysis, *IEEE Transactions on Geoscience and Remote Sensing*, 44, 1297-1307, 10.1109/TGRS.2006.871234, 2006.
- Deeter, M. N., Edwards, D. P., Francis, G. L., Gille, J. C., Martínez-Alonso, S., Worden, H. M., and Sweeney, C.: A climate-scale satellite record for carbon monoxide: the MOPITT Version 7 product, *Atmos. Meas. Tech.*, 10, 2533-2555, 10.5194/amt-10-2533-2017, 2017.
- Deeter, M. N., Martínez-Alonso, S., Edwards, D. P., Emmons, L. K., Gille, J. C., Worden, H. M., Pittman, J. V., Daube, B. C., and Wofsy, S. C.: Validation of MOPITT Version 5 thermal-infrared, near-infrared, and multispectral carbon monoxide profile retrievals for 2000–2011, *Journal of Geophysical Research: Atmospheres*, 118, 6710-6725, <https://doi.org/10.1002/jgrd.50272>, 2013.
- Herman, R. and Kulawik, S.: Tropospheric Emission Spectrometer TES Level 2 (L2) Data User's Guide, D-38042, version 6.0, Jet Propulsion Laboratory, California Institute of Technology, Pasadena, CA, available at: <http://tes.jpl.nasa.gov/documents> (last access: 30 June 2014), 2013.
- KOFFI, L. B., DENTENER, F., JANSSENS-MAENHOUT, G., GUIZZARDI, D., CRIPPA, M., DIEHL, T., GALMARINI, S., and SOLAZZO, E.: Hemispheric Transport of Air Pollution (HTAP): Specification of the HTAP2 experiments: Ensuring harmonized modelling, 2016.
- Krotkov, N. A., McLinden, C. A., Li, C., Lamsal, L. N., Celarier, E. A., Marchenko, S. V., Swartz, W. H., Bucsela, E. J., Joiner, J., and Duncan, B. N.: Aura OMI observations of regional SO₂ and NO₂ pollution changes from 2005 to 2015, *Atmospheric Chemistry and Physics*, 16, 4605-4629, 2016.
- Li, C., Joiner, J., Krotkov, N. A., and Bhartia, P. K.: A fast and sensitive new satellite SO₂ retrieval algorithm based on principal component analysis: Application to the ozone monitoring instrument, *Geophysical Research Letters*, 40, 6314-6318, <https://doi.org/10.1002/2013GL058134>, 2013.

Livesey, N., Read, W., Wagner, P., Froidevaux, L., Lambert, A., Manney, G., Valle, L., Pumphrey, H., Santee, M., and Schwartz, M.: Version 4.2 x level 2 data quality and description document, JPL D-33509 Rev, 2017.